Ultramicroscopy 000 (2017) 1–11

Contents lists available at ScienceDirect

Ultramicroscopy

journal homepage: www.elsevier.com/locate/ultramic

Excitonic, vibrational, and van der Waals interactions in electron energy loss spectroscopy

T. Mizoguchi[a,*], T. Miyata[a], W. Olovsson[b]

[a] Institute of Industrial Science, University of Tokyo, Tokyo 153-8505, Japan
[b] Department of Physics, Chemistry and Biology (IFM), Linköping University, SE-581 83 Linköping, Sweden

ARTICLE INFO

Article history:
Received 19 October 2016
Revised 21 February 2017
Accepted 1 March 2017
Available online xxx

Keywords:
Excitonic interaction
Li-ion battery
van der Waals interaction
Vibrational information
Gas and liquid
First principles calculation

ABSTRACT

The pioneer, Ondrej L. Krivanek, and his collaborators have opened up many frontiers for the electron energy loss spectroscopy (EELS), and they have demonstrated new potentials of the EELS method for investigating materials. Here, inspired by those achievements, we show further potentials of EELS based on the results of theoretical calculations, that is excitonic and van der Waals (vdW) interactions, as well as vibrational information of materials. Concerning the excitonic interactions, we highlight the importance of the two-particle calculation to reproduce the low energy-loss near-edge structure (ELNES), the Na-$L_{2,3}$ edge of NaI and the Li-K edge of LiCl and $LiFePO_4$. Furthermore, an unusually strong excitonic interaction at the O-K edge of perovskite oxides, $SrTiO_3$ and $LaAlO_3$, is shown. The effect of the vdW interaction in the ELNES is also investigated, and we observe that the magnitude of the vdW effect is approximately 0.1 eV in the case of the ELNES from a solid and liquid, whereas its effect is almost negligible in the case of the ELNES from the gaseous phase owing to the long inter-molecular distance. In addition to the "static" information, the influence of the "dynamic" behavior of atoms in materials to EELS is also investigated. We show that measurements of the infrared spectrum are possible by using a modern monochromator system. Furthermore, an estimation of the atomic vibration in core-loss ELNES is also presented. We show the acquisition of vibrational information using the ELNES of liquid methanol and acetic acid, solid Al_2O_3, and oxygen gas.

1. Introduction

Electron energy loss spectroscopy (EELS) observed with transmission electron microscopy (TEM) has been extensively used in diverse fields, such as materials science, solid state physics, biological chemistry, and polymer chemistry [1]. The reason for this wide range of applications is attributed to the numerous advantages of the TEM-EELS method. The most important advantage is its high spatial resolution. EELS observation with very high spatial resolution has been achieved more than twenty years ago by the combination of EELS with a scanning transmission electron microscope (STEM) [2–5]. To date, some milestones for the atomic resolution analysis using STEM have been recorded by a pioneer, Ondrej L. Krivanek, and his collaborators and the instruments developed by them [6–11]. In 2010, the ultimate resolution, that is atom-by-atom analysis, was achieved [11].

In addition to the spatial resolution, the wide variety of information obtainable from an EELS spectrum is also an important advantage of the EELS method. Information on the chemical composition of a sample can be obtained by from the fine-structure of its core-loss EEL spectrum. The spectral profile and threshold energy of ELNES are known to be sensitive to the local coordination, valence state, and chemical bonding. A lower energy profile of the EELS spectrum also contains important information on the material. The low loss profile originates from phonons, collective electron oscillations, as well as the inter and intra band transitions, and thus, optical properties can be measured using low loss EELS [1,12]. With a modern aberration-corrected STEM system, atomic resolution observation of the spectrum from a single dopant [9], two-dimensional mapping of elements in a bulk [13] and at a interface [14], dopant buried in a crystal [15], and valence state mapping [16], are all possible. Some of these cutting-edge observations have been performed by the instruments developed by the group of Krivanek and coworkers [9,14].

Furthermore, new techniques in EELS have also been developed recently. The observation of magnetic circular dichroism using ELNES has been achieved using a vortex electron beam [17–19]. More recently, an improvement of the energy resolution, via the development of an advanced monochromator system, enables

* Corresponding author.
E-mail address: teru@iis.u-tokyo.ac.jp (T. Mizoguchi).

http://dx.doi.org/10.1016/j.ultramic.2017.03.003
0304-3991/

the identification of fine profiles near the zero-loss peak [20–23], as described in a review [24]. An instrument that is compatible for both advanced spatial resolution and energy resolution has also been developed by Krivanek et al. [25–27]. The advanced energy resolution enables us to provide information on the electronic structure at the band gap (gap between the highest occupied molecular orbital (HOMO) and the lowest unoccupied molecular orbital (LUMO)) and the vibration of atoms in the molecule and solid [25,28,29].

Nowadays, the TEM/STEM-EELS method is a very informative and powerful analytical technique for a wide variety of scientific fields. Significant pioneering contributions were made by Ondrej L. Krivanek to open up these frontiers, as described above. Based on this background, we would like to show further potential applications of EELS, based on the results of theoretical calculations. In this study, we discuss 1) excitonic interactions in ELNES, 2) effect of van der Waals interactions in ELNES, and 3) vibrational information from EELS.

The excitonic interaction is known to be significant in ELNES in the relatively lower energy region, <100 eV [30–35], whereas its effect on the high energy ELNES is still a cause of controversy [32,36]. We have investigated the excitonic interactions in the low energy ELNES, Na-$L_{2,3}$ edge (~30 eV) of NaI and the Li-K edge (~50 eV) of LiCl [37], as well as the high energy ELNES at the O-K edge (~530 eV) of perovskite oxides [36]. Here, we review those results, and an application of the excitonic calculation is also shown for the Li-K edge and Fe-$M_{2,3}$ edge of a Li-ion battery cathode material, $LiFePO_4$, and the importance of correct calculation of the transition energy is demonstrated.

Concerning the van der Waals (vdW) interaction, it is known that one of its constituents, the London dispersion force, can be estimated from the plasmon loss [38]. However, the effect of the vdW interaction in core loss, ELNES, has not been discussed. We have investigated the effect of the vdW interaction on the B-K edge of solid h-BN, the O-K edge of liquid water, and the O-K edge of a gas water molecule using first-principles calculations [39].

In addition to the above "static" information, we investigated the "dynamic" behavior of atoms in materials, such as phonons and molecular vibrations, in the EELS spectrum. Direct observation of the vibrational spectrum using monochromated STEM-EELS from an ionic liquid, C_2mim-TFSI, has been reported [29]. Furthermore, we have also reported the effects of the molecular vibration on the liquid ELNES, C-K edge of liquid methanol and O-K edge of acetic acid [40,41]. Here, in addition to those previous results, we show the effect of the lattice/molecular vibration on the Al-K edge of solid Al_2O_3 and O-K edge of oxygen gas.

2. Excitonic interactions in ELNES

The features of ELNES originate from an electron transition from a core-orbital to the conduction bands. Here, the "ground state" is defined as the state before the electron transitions and the state with a core-hole is called an "excited state". At the excited state, a Coulombic interaction between the positively charged core-hole and the negatively charged excited electron, namely an excitonic interaction, is present.

To investigate the excitonic interaction, a correct calculation of the two-particle formalism, namely the Bethe–Salpeter equation (BSE), is necessary [30,31,33,34]. The method to calculate the excitonic interaction using BSE is provided next.

2.1. Methodology for the excitonic calculation

To investigate the excitonic interaction, both the one-particle and two-particle calculations were performed. In the one-particle calculations, the electron-hole interaction is treated under the generalized gradient approximation (DFT-GGA). Namely, the particle–particle interactions are approximated to be interactions between an electron and the mean field generated by other particles. Hereafter, we will name the one-particle calculation as "DFT-GGA". In DFT-GGA, one core-hole is introduced into the respective core-orbital, and the electronic structure at the excited state is calculated. To minimize the artificial interactions between core-holes, a large supercell was used. The theoretical transition energy was also calculated in the one-particle calculation by the total energy difference between the excited state and ground state [35].

In the two-particle calculation, the BSE calculation was performed to accurately consider the two-particle (electron–hole) interactions. The effective two-particle Hamiltonian with spin-orbit interaction, which treats the excitonic effect, is described as:

$$H^{eh} = H^{diag} + H^{dir} + H^{x}, \quad (1)$$

where H^{diag}, H^{dir}, and H^{x} are the diagonal term, the direct term, and the exchange term, respectively [31].

To calculate the BSE, the one-particle wave functions obtained from the DFT-GGA calculation were used in this study. Hereafter, we will name the two-particle calculation "BSE-GGA". However, this BSE-GGA method has a disadvantage in that it cannot estimate the theoretical transition energy [42]. A correct estimation of the theoretical transition energy becomes important when a spectrum is overlapped or very close to another spectrum. For instance, the Li-K edge of Li-ion battery cathode materials always encounters this problem. The cathode materials usually include both Li and 3d transition metals (TM), and the position of the Li-K edge and the TM-$M_{2,3}$ edge are very similar. In such a case, the theoretical transition energy must be estimated separately using the DFT-GGA method.

In the present study, we used suitable calculation codes depending on the purpose. First-principles all-electron calculation codes based on the augmented plane wave and local orbital (APW+lo) method, WIEN2k code [43], and a full-potential linearized augmented plane wave (FLAPW) method, and the Elk code were used for the one-particle calculations [43,44]. All the BSE-GGA calculations were performed using the Elk code. To correctly calculate the spectra, the size of the supercell, number of k-points, and the cutoff energy of the plane wave were carefully chosen.

2.2. Low energy ELNES

The excitonic interaction is known to be significant for a relatively lower energy ELNES, because the core-hole and the excited electron are energetically and spatially close to each other. For instance, the Li-K and Na-$L_{2,3}$ edges appear around 50 eV and 30 eV, respectively, and thus, the excitonic interaction is expected to be significant. To show the strong excitonic interaction in the low energy ELNES, the Na-$L_{2,3}$ edge of NaI and Li-K edge of NaCl were investigated.

The Na-$L_{2,3}$ edges of NaI are shown in the Fig. 1(a). The experimental spectrum was determined using X-rays in a previous report [45]. As can be seen in the figure, the experimental spectrum shows an intense excitonic peak B which is followed by a small peak, a relatively intense peak, and a plateau profile. These characteristic features appear in both the BSE-GGA and DFT-GGA calculations. Furthermore, the small splitting in peak B can only be reproduced when spin–orbit coupling is considered. However, a detailed investigation shows that the position of peak B is overestimated by DFT-GGA. However, the BSE-GGA calculations correctly reproduced the position. A similar overestimation of the excitonic peak position with DFT-GGA has also been observed for the Li-K edge of Li compounds [35]. The experimental and calculated Li-K edge of LiCl are also shown in Fig. 1(b). The calculated spectra us-

Please cite this article as: T. Mizoguchi et al., Excitonic, vibrational, and van der Waals interactions in electron energy loss spectroscopy, Ultramicroscopy (2017), http://dx.doi.org/10.1016/j.ultramic.2017.03.003

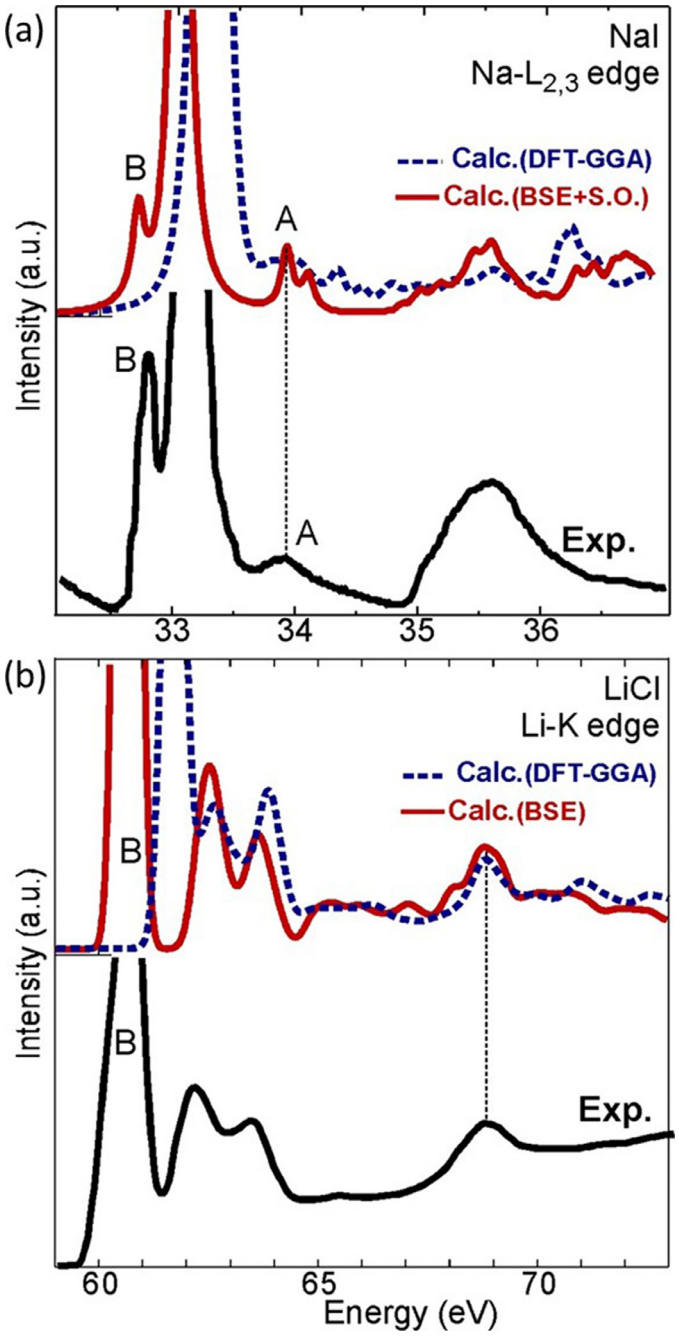

Fig. 1. (a) Calculated and experimental Na-$L_{2,3}$ edge of NaI [37,45]. The experimental spectra were observed using X-rays [45]. The calculations using DFT-GGA and BSE-GGA are shown. To reproduce the L_3-L_2 splitting in peak B, the spin-orbit coupling (S.O.) was considered in the BSE-GGA calculation. (b) Calculated and experimental Li-K edge of LiCl [35].

ing both the DFT-GGA and BSE-GGA methods are shown. To reproduce the excitonic peak A, the BSE-GGA method is indispensable. These results indicate that the excitonic interaction between the hole at the core orbitals and the excited electron is strong at the Na-$L_{2,3}$ and Li-K edges, and thus, the two-particle method is critical to reproduce the experimental spectrum. However, the present BSE-GGA method has a disadvantage compared with the DFT-GGA method, in that the BSE-GGA method cannot estimate the transition energy. This becomes critical when we investigate the ELNES from cathode materials of a Li-ion battery. This point is further discussed in the next section.

2.3. Li-K edge of Li-ion battery cathode materials

Since Li and Na are important elements for battery applications, the ELNES observation of these materials have been investigated [46–51]. However, the interpretation of the ELNES from battery materials is always accompanied by difficulties because such materials usually contain a 3d transition metal (TM). The $M_{2,3}$ edge of TM appears around 20 eV–70 eV, which overlaps with the Li-K and Na-$L_{2,3}$ edges. This overlap often makes identification of the ELNES difficult. For instance, Fig. 2(b) shows the experimental Li-K and Fe-$M_{2,3}$ edges of $LiFePO_4$ [46]. The spectrum of $LiFePO_4$ has extra features both at the lower and higher energy sides, as shown by the arrows, and these features disappear (or are reduced) for the charged $FePO_4$ (Fig. 2(b)). Since the energy range of both the Li-K edge and Fe-$M_{2,3}$ edge are similar, a discrimination of their features is not straightforward.

To investigate the spectrum, the electronic structure of $LiFePO_4$ is assessed, with Fig. 2(a) showing the density of states (DOS) of $LiFePO_4$. Since the conventional $LiFePO_4$ contains 28 atoms in the unit cell, the calculation using BSE-GGA is computationally difficult. Therefore, we used a simplified $LiFePO_4$ structure for the BSE-GGA calculation [52]. Although a simplified structure was used, the local coordination environments of Li, Fe, and P were similar to the ideal $LiFePO_4$, and the number of atoms in the unit cell was 14 atoms, which enables us to perform the BSE-GGA calculation. It can be seen that the Li-1s and Fe-$3p_{3/2,1/2}$ semi-core states are located at −41.5 eV and −51.5 eV, respectively. Since the Li-K and Fe-$M_{2,3}$ edges originate from the electron transition from the Li-1s and Fe-3p states to the conduction band, respectively, it can be expected that the Li-K edge should appear on the lower energy side of the Fe-$M_{2,3}$ edge from the result of the DOS.

The calculated Li-K and Fe-$M_{2,3}$ edges using BSE-GGA are shown in Fig. 2(b) Although we know that consideration of multi-particle interactions is important for the Fe-$M_{2,3}$ edge [53,54], the two-particle calculation, BSE-GGA, was used in this study to simply investigate the characteristic features and position of the spectral threshold. As can be seen from Fig. 2(b), the Li-K edge appears below the Fe-$M_{2,3}$ edge. In this BSE-GGA method, the energy positions reflect the results of the DOS. This result implies that the profiles at the lower energy side of the Fe-$M_{2,3}$ edge is caused by the Li-K edge. However, as mentioned above, this BSE-GGA method cannot estimate the transition energy, and thus we have to confirm the correct position of the edges.

To confirm the relative energy positions, the theoretical transition energy was separately calculated using the total energy difference between the ground state and excited state using DFT-GGA. Although the DFT-GGA method is a one-particle method, it can be used to estimate the transition energy qualitatively because DFT can correctly calculate the total energy [35,43,55–57]. The calculated transition energy of the Li-K and Fe-$M_{2,3}$ edges, using the DFT-GGA method, were 54.3 eV and 48.4 eV, respectively. Fig. 2(c) shows the calculated spectra with the correct transition energy. The Li-K edge appears at the higher energy side of the Fe-$M_{2,3}$ edge. Namely, this combined calculation method, using BSE-GGA and DFT-GGA, shows that the features at the higher energy side originate from the Li-K edge. This change in the order of the spectral position is ascribed to the core-hole effect of the Li-K edge being stronger than that of the Fe-$M_{2,3}$ edge.

These results demonstrate that the excitonic calculation is indispensable for the interpretation of the low energy ELNES. Furthermore, a correct calculation of the transition energy is also important when the spectrum overlaps with another spectrum.

Please cite this article as: T. Mizoguchi et al., Excitonic, vibrational, and van der Waals interactions in electron energy loss spectroscopy, Ultramicroscopy (2017), http://dx.doi.org/10.1016/j.ultramic.2017.03.003

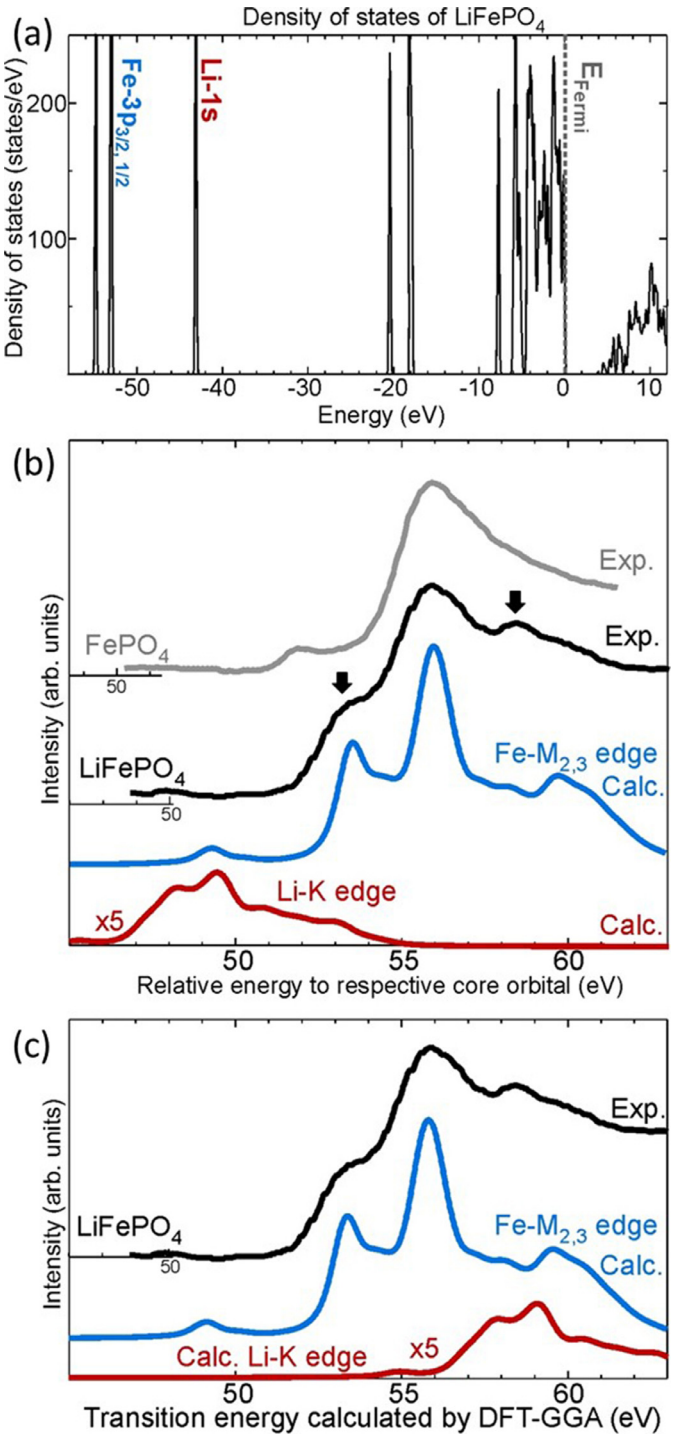

Fig. 2. (a) Calculated density of states of $LiFePO_4$ using GGA+U. (b) Experimental [46] and calculated Li-K and Fe-$M_{2,3}$ edges of $LiFePO_4$. The positions of the calculated spectra were determined using the relative energy to the respective core-orbital. (c) The calculated transition energy determined by separately performing DFT-GGA calculation.

2.4. High energy ELNES

Since the excitonic interaction arises from the Coulombic interaction between the core-hole and the excited electron, it is generally considered that their interaction becomes strong when they are energetically and spatially close to each other, namely for the low energy ELNES, whereas it can be expected that the excitonic interaction is weak for the high energy ELNES. Actually, the excitonic interaction of the O-K (~535 eV) and Mg-K (~1350 eV) edges of MgO have been investigated by BSE-GGA, and it was concluded that the excitonic interactions for these high energy ELNES are negligible [32]. However, the presence of a strong excitonic interaction in the O-K edge of perovskite oxides has recently been demonstrated by the group of Tomita et al. [36]. Below, in addition to the results reported in the previous report [36], a new result for $LaAlO_3$ is shown.

Fig. 3(a) and (b) show the experimental and calculated oxygen K-edge of MgO and perovskite type $SrTiO_3$. Both the calculated spectra using the BSE-GGA and DFT-GGA methods are shown. In the MgO case, both BSE-GGA and DFT-GGA provided almost identical features and both methods reproduced the experimental spectrum [32,58]. However, in the case of $SrTiO_3$, a detailed inspection showed some differences between the experimental spectrum and the calculated spectrum using DFT-GGA. The distance between peaks A and C in the experimental spectrum was 5.2 eV, whereas it was 4.1 eV in the spectrum calculated using DFT-GGA, that is, a 1.1 eV error was present in the DFT-GGA calculation. Furthermore, peak B was less intense in the DFT-GGA calculation than in the experimental spectrum. Although the consideration of the effect of the elastic and thermal scattering to the spectral profile is important [59–61], it was confirmed that the peak positions are not changed much by the inversion process, indicating that the disagreement between the experiment and the GGA calculation is not caused by the effect of the elastic and thermal scattering [36]. Conversely, the BSE-GGA calculation reproduced the A–C peak distance and small peak B well. This result suggests that, contrary to the case of MgO, the excitonic interaction in the oxygen K-edge of $SrTiO_3$ is not negligible and, thus, the BSE-GGA calculation is necessary to reproduce the fine profile of the experimental spectrum. A similar trend was observed for $CaTiO_3$ and $BaTiO_3$ [36].

In addition to the titanate perovskite oxides, we observed a similar behavior in $LaAlO_3$. Fig. 3(c) shows the experimental and calculated oxygen K-edge of $LaAlO_3$. Similar to the titanate perovskite oxides, the B–C peak distance was underestimated by the DFT-GGA calculation, whereas it was well reproduced in the BSE-GGA calculation.

The origin of this unusually strong excitonic interaction in the O-K edge of perovskite materials was investigated and it was concluded that it is caused by directionally confined Ti(Al)–O–Ti(Al) bonds formed in the perovskite oxides [36].

3. Effect of van der Waals interactions on ELNES

The van der Waals (vdW) interaction is a weakly attractive or repulsive force between molecules or groups of atoms that do not arise from covalent or ionic bonds. The vdW interaction is known to be a generic name for the following three forces: 1) force between permanent dipoles (Keesom force), 2) force between a permanent dipole and a corresponding induced dipole (Debye force), and 3) force between instantaneously induced dipoles (London dispersion force). The vdW interaction is known to play an important role on the electronic structure of two-dimensional layered structure materials and molecular crystals and on the stability of the crystal phase [62]. However, the effect of the vdW interaction in the ELNES feature has not been considered to date, because the spectral change arising from the vdW interaction has been believed to be below the measurable limit owing to its much smaller influence than that of ionic and covalent bonding. However, the vdW interaction is present in every material and the identification of it using ELNES is greatly beneficial especially for investigating the vdW interaction at a local region such as an interface and a surface. We investigated the effect of the vdW interaction on first-principles ELNES calculations, and discussed the spectral changes that are generated from the vdW interaction. Since the vdW effect

Please cite this article as: T. Mizoguchi et al., Excitonic, vibrational, and van der Waals interactions in electron energy loss spectroscopy, Ultramicroscopy (2017), http://dx.doi.org/10.1016/j.ultramic.2017.03.003

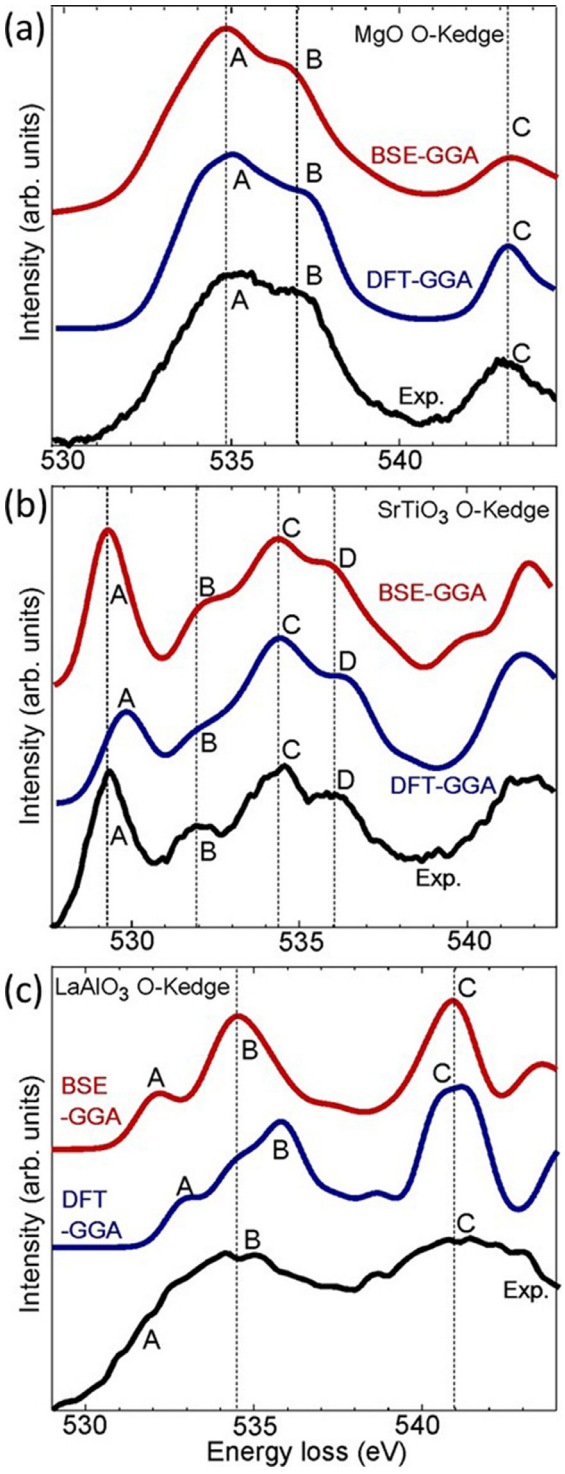

Fig. 3. Experimental [73–75] and calculated O-K edge of (a) MgO, (b) $SrTiO_3$, and (c) $LaAlO_3$. Both calculated spectra using BSE-GGA and DFT-GGA are shown.

differs depending on the state, the influence of the vdW interaction on ELNES calculations of solid h-BN, liquid water, and gaseous water were systematically investigated.

3.1. Methodology

To introduce the vdW interaction into the ELNES calculation, we applied the semi-empirical vdW-TS approach of Tkatchenko and Scheffler [63], which is implemented in the CASTEP code [64]. This method corrects the DFT energy by adding the following term:

$$E_{\mathrm{vdW}} = -\frac{1}{2}\sum_{B} f_{damp}(R_{AB}) C_{6AB}^{\mathrm{eff}} R_{AB}^{-6} \tag{2}$$

where $f_{damp}(R_{AB})$ is the damping function preventing the vdW energy, E_{vdW}, from diverging at a short atomic distance. R_{AB} is the distance between atoms A and B. C_{6AB}^{eff} is the effective dispersion coefficient expressed using C_{6AA}^{free} and C_{6BB}^{free}, which are homonuclear coefficients reported by Chu and Dalgarno [65] and the Hirshfeld volume of atom A(B) [66], which is calculated from the total electron density, $n(\mathbf{r})$, of the isolated atom and molecule.

The electronic structure and ELNES spectra of these models were calculated using the first-principles DFT plane-wave basis pseudopotential method within the CASTEP code [64]. The exchange-correlation functional was approximated by GGA-PBE [67]. The plane-wave cutoff energy was set to 500 eV. In the ELNES calculation, $1 \times 1 \times 1$ k-point sets for the liquid and gaseous structures, and $2 \times 2 \times 1$ k-point sets for the solid structures were used because the size of the supercells was sufficiently large.

To introduce the core-hole effects, an excited pseudopotential was separately generated for the electronic configuration obtained by removing one electron from the core orbital. To maintain charge neutrality, one electron was placed onto the bottom of the conduction band. The core-orbital was obtained from an all-electron calculation of an isolated atom. In the calculation of the theoretical transition energy (E_{TE}), the contribution of the core-orbitals to the total energy was approximated by the all-electron calculation of an isolated atom [68]. This approximation method can reproduce the amount of the chemical shift quantitatively [35,39–41,68,69].

3.2. vdW interactions in solid, liquid, and gas ELNES

Fig. 4(a)–(c) shows the experimental and calculated ELNES of solid h-BN, liquid water, and gaseous water, respectively. Both the calculated spectra with and without consideration of the vdW interaction are shown. As can be observed in the figure, irrespective of the consideration of the vdW interaction in the calculation, both the calculated spectra reproduced the overall profile of the experimental spectrum. However, a detailed inspection revealed that the peaks in the h-BN and water commonly shift to lower energies by approximately 0.1 eV when the vdW interaction is considered, whereas no changes were observed in the calculated spectra of the gas model. The transition energy TE(with vdW) is defined as the total energy difference between the excited state and the ground state with the vdW interaction, whereas TE(without vdW) is that without the vdW interaction. Therefore, the difference of the transition energy by introducing the vdW interaction (ΔTE) is given by:

$$\Delta\mathrm{TE} = \mathrm{TE}(\text{with vdW}) - \mathrm{TE}(\text{without vdW}) = \Delta\mathrm{ES} - \Delta\mathrm{GS} \tag{3}$$

where ΔGS is the total energy difference between the ground state (GS) with and without the vdW interaction, while ΔES corresponds to that between the excited state (ES). A detailed inspection of the total energies at the ground and the excited states revealed that the vdW interaction influences the excited state more than the ground state [39].

The reason the vdW interaction exhibits more influence on the excited state can be understood from the localization of the electron. A larger and more delocalized electron density is affected to a greater extent by the vdW interaction. At the excited state, the position of an electron transfers from the core-orbital to the unoccupied band, which leads to the generation of a core-hole. The core-orbital is significantly localized at the nucleus, whereas the unoccupied band is more delocalized than the core-orbital even in the excited state. This electron transition (transfer) process from the localized core-orbital to the relatively delocalized unoccupied

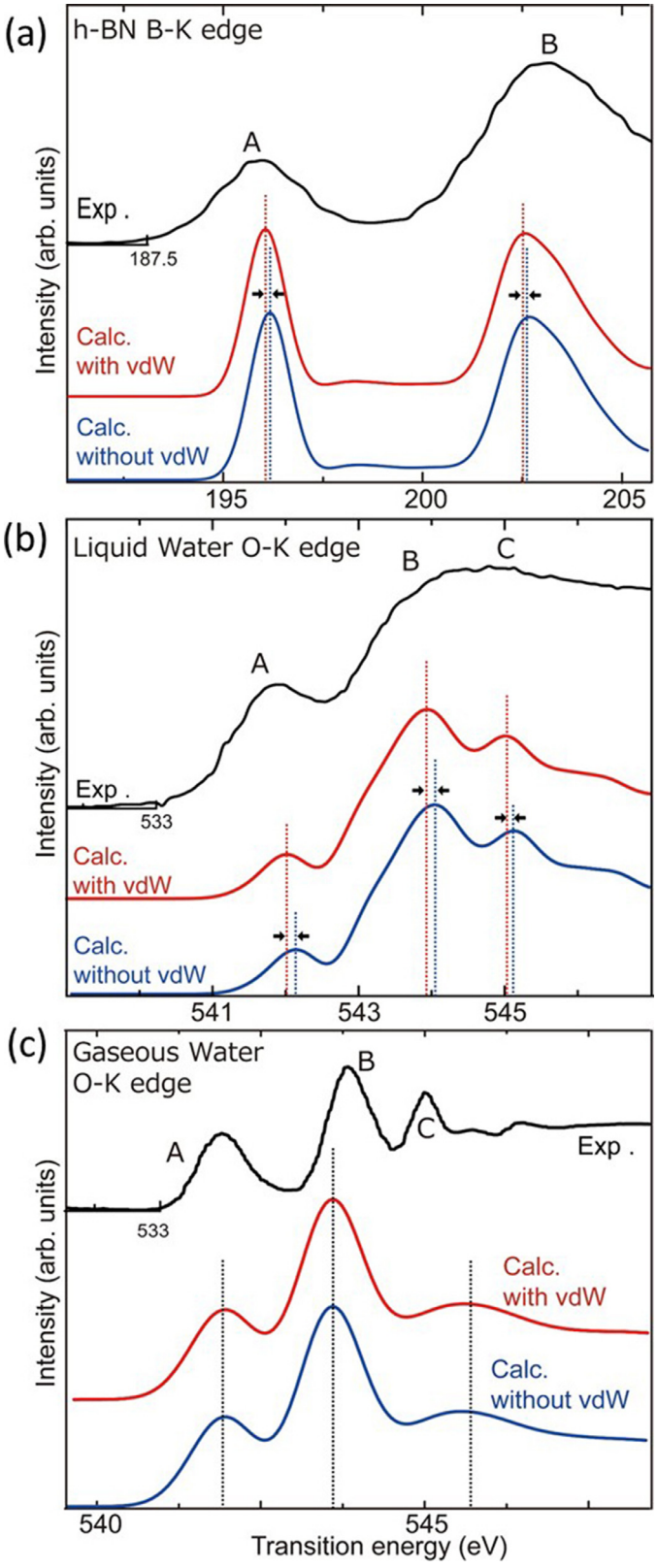

Fig. 4. Effect of van der Waals interactions to the ELNES of (a) B-K edge of solid h-BN, (b) O-K edge of liquid water, and (c) O-K edge of gaseous water. The experimental spectra were obtained from the literature [76–78].

band is the origin for the stronger vdW interaction of the excited state.

In contrast to the spectral shifts in the ELNES observed for solid h-BN and liquid water, the effect of the vdW interaction was almost zero in gaseous water (Fig. 4(c)). As can be understood from Eq. (2), the vdW effect is dominated by R_{AB}^{-6}. Namely, the effect of the vdW interaction on the gaseous ELNES is negligible because of the large intermolecular distance.

These results suggest that the effect of the vdW interaction on the ELNES is approximately 0.01–0.1 eV. This influence is almost negligible and cannot be identified using the conventional (traditional) TEM-EELS equipment. However, the energy resolution and stability of the instruments have rapidly been improved. We believe that identification of the vdW interaction by ELNES will be possible owing to the further development of instruments, which will pave the way for identification of the vdW interaction with a high spatial resolution.

4. Vibrational information in EELS

4.1. Infrared region

In this section, the information on the vibrational behavior of atoms in molecules or solids in EELS is discussed. In general, the vibrational information, such as molecular vibrations and phonons, is known to appear in the very low energy region, <0.5 eV. To observe such a spectrum in the very low energy region, dedicated instruments, such as infrared (IR) and Raman, have been used. However, the energy resolution of EELS has dramatically been improved owing to the development of the monochromator [22,25,29]. By using the modern monochromator system, one can achieve an energy resolution of several tens of meV or better. This enables us to observe the infrared spectrum directly using the TEM-EELS equipment.

In our experiment, a two stage Wien filter monochromator system (JEOL 2400FCS) equipped with a high energy resolution spectrometer (Tridiem ERS, Gatan) operated at 60 keV was used. The IR spectrum of an ionic liquid (1-ethyl-3-methylimidazolium bis-(trifluoromethyl-sulfonyl) imide, C_2mim-TFSI) was obtained. The molecule structure is shown in Fig. 5(a). Since the ionic liquid is non-vaporized even under vacuum, separation membranes, such as SiN and graphene, are not necessary for the present experiment. This provides a great advantage for the acquisition of a high quality spectrum.

Fig. 5(b) shows the EEL spectrum near the zero-loss peak. In the EELS observation, the beam current at the specimen was 48 pA and that at the spectrometer was around 0.72 pA. The EEL spectrum was taken using a 0.6 nm electron probe, and the acquisition time was 10.0 s. By magnifying the EEL spectrum, a small shoulder could be confirmed at approximately 0.4 eV. The relative intensity of this shoulder to the zero-loss peak was approximately 1/250, and its profile was extracted by subtracting the background, which yielded a characteristic peak at around 0.4 eV. For comparison, the experimental and calculated IR spectra of C_2mim-TFSI are shown in the same figure. The calculation was performed using a first-principles plane-wave basis pseudopotential method, CASTEP code, and the present calculation correctly reproduced the experimental IR spectrum. The peaks around 0.35 eV–0.4 eV (2800 cm^{-1}–3200 cm^{-1}) were caused by the C–H stretching vibrations in the cation molecule, as schematically shown using the green arrows in Fig. 5(a), for instance [29]. The vibrational spectrum of solid materials obtained by monochromated electron microscopy has also been reported by Krivanek et al. [25]. More recently, Crozier et al. and Rez et al. reported an effective method to observe the vibrational spectrum for electron-beam damage-sensitive specimens [70,71].

Please cite this article as: T. Mizoguchi et al., Excitonic, vibrational, and van der Waals interactions in electron energy loss spectroscopy, Ultramicroscopy (2017), http://dx.doi.org/10.1016/j.ultramic.2017.03.003

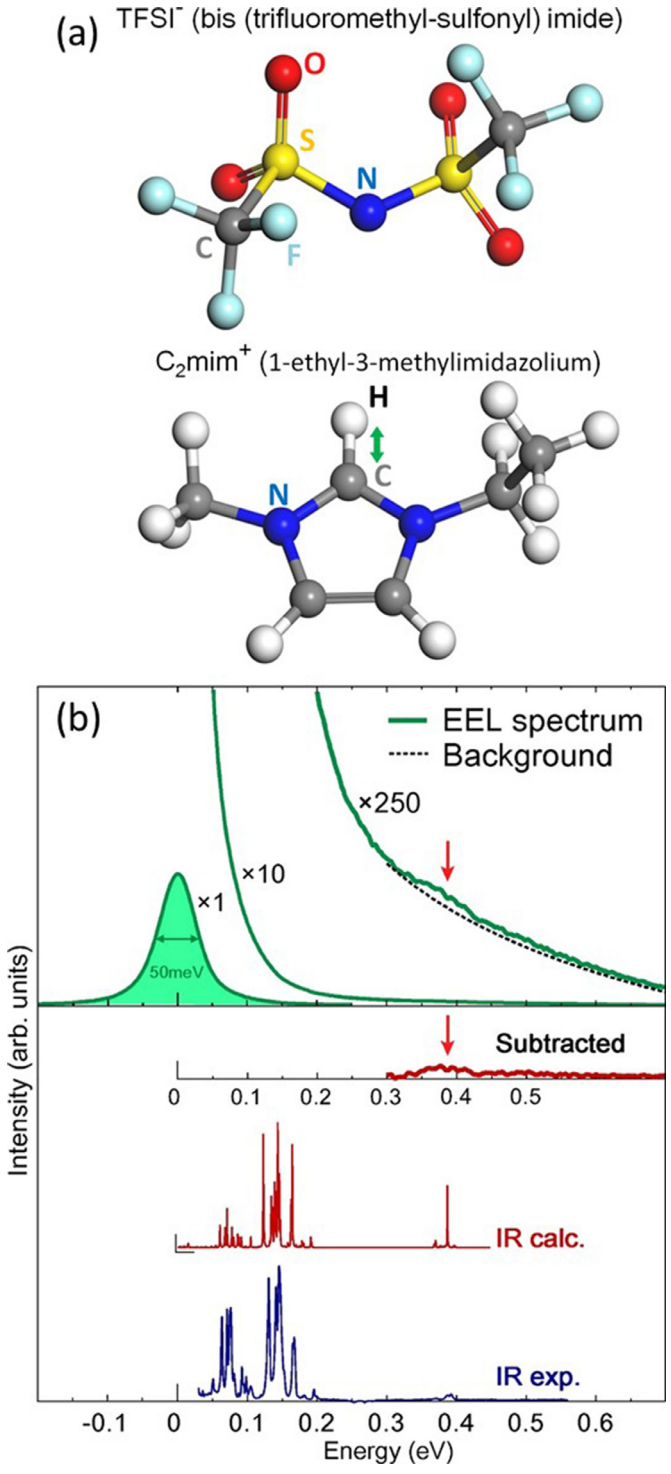

Fig. 5. (a) Molecular structure of the ionic liquid, C_2mim-TFSI. $TFSI^-$ and C_2mim^+ are the anion and cation molecules, respectively. (b) Experimental and calculated spectra of the infrared region [29].

As presented here, the vibrational information is directly observed using a modern monochromator system. However, the vibrational behavior of atoms in materials also influences the ELNES profile. The identification of the dynamic behavior of atoms in materials using ELNES is discussed in the next section.

4.2. Effect of vibrational information in ELNES

In this section, the identification of the vibrational information using core-loss, namely ELNES, of a liquid, solid, and gaseous phase are discussed. The effect of the atomic vibrations, such as molecular vibrations or phonons, should influence the ELNES features based on a consideration of the time scales for each phenomenon. Namely, the time scale of electron excitation is on the order of sub-femtoseconds ($\sim 10^{-16}$ s), whereas that of atomic vibrations (phonons) is on the order of sub-nano- to sub-picoseconds (10^{-10}–10^{-13} s). Furthermore, the exposure time used to measure the core-loss spectrum is typically much longer, on the order of milliseconds or tens of seconds (10^{-3}–10 s). On the electron-transition time scale, the molecular vibration appears as a (very slow) frame-by-frame advance of snapshots, and the interactions between one snapshot and the other snapshots can be neglected. In this case, the ELNES should reflect the average spectrum for multiple snapshots. Hereafter, we discuss the observation of the vibrational information using ELNES.

4.2.1. Vibrational information in ELNES of a liquid

In this section, the vibrational information in core-loss ELNES from liquid methanol is presented. The calculated and experimental C-K edge of liquid methanol is shown in Fig. 6(a). To include the liquid structure, a molecular dynamics (MD) simulation of the liquid model, which includes 16 methanol molecules, was performed. Then, a single snapshot was taken from the MD simulation and the spectrum from all carbon atoms in the liquid model were calculated. These spectra were averaged for comparison with the experimental spectrum. The obtained spectrum using the MD simulation at 313 K is shown in Fig. 6. The experimental spectrum was obtained from the Operand-XAFS observation at 298 K. The C-K edge of liquid methanol is composed of pronounced peaks A and B at the spectral threshold which are followed by broad peak C. It is observed that the calculated spectrum agrees well with the experimental spectrum.

Two other spectra from the liquid models were constructed from the 253 K and 193 K MD simulations, and they are compared in the same figure. Although the overall profiles were similar with each other, that is, the pronounced A and B peaks appear at the threshold followed by a broad C peak, a detailed inspection showed a clear spectral change in which peaks A and B approached one another as the temperature was decreased. By investigating the liquid models at various temperatures, it was found that the changes in the separation of peaks A and B is caused by the changes in the C–O bond length during the MD simulations. Namely, the molecular vibrations of the molecules in the liquid are more intense at high temperatures, so the peak A-B splitting increases [41].

Similar investigation was performed for O-K edge of liquid acetic acid (Fig. 6(b)). The acetic acid has two kind of oxygen sites, one is connected by single bonding and another is by double bonding with carbon. The liquid model containing 10 molecules was constructed by the MD simulation at 293 K and O-K edge spectra were separately calculated from all oxygens. Detailed investigation revealed that peak A originates from the oxygen that has a double bond, whereas the single-bonded oxygen contributes to peak B, and peak C results from both oxygens [40]. Although the overall features were reproduced by the gas model, the gas model cannot reproduce the details of the spectrum. In particular, peak B is broader than peak A in the experiment whereas the calculated peak B shows a similar intensity as peak A in the gas model calculation. Furthermore, the A-B peak separation is 2.2 eV in the experiment, whereas it is 2.7 eV in the gas model calculation. A theoretical calculation of the liquid model was performed to achieve better agreement between theory and experiment. Furthermore,

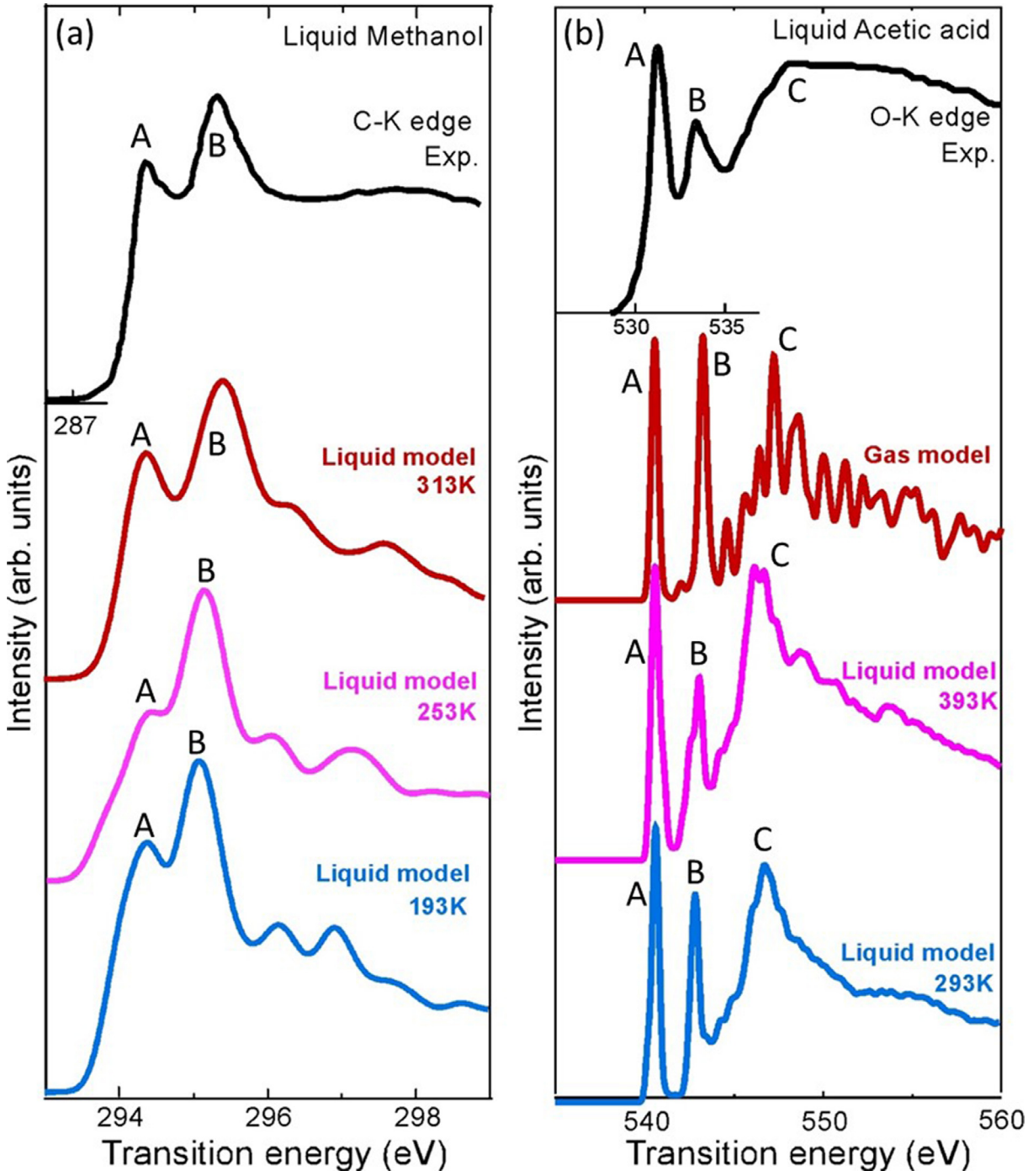

Fig. 6. (a) Experimental and calculated C-K edge of liquid methanol and (b) O-K edge of liquid acetic acid. The calculated spectra with different temperatures are also shown [40,41]. The experimental spectra were observed using X-rays [79,80].

another MD simulation at 393 K was also performed and the averaged spectrum simulated at 393 K is shown in the same figure. As can be seen in the calculated spectra, peak B becomes less intense and broader than that at 293 K. The variety of C–O bond lengths in the liquid model at 393 K is larger than that in 293 K, indicating that the larger variety of peak feature is generated [40].

Through this result, the relationship between the vibrational behavior of the molecules in a liquid and its core-loss spectrum is revealed. The basis for the dynamic information in the core-loss spectrum is the large differences in the time scale for each phenomenon, as described above. This vibrational information in ELNES is available by combination with suitable spectral calculations.

4.2.2. Vibrational information in ELNES of a solid: effect of temperature

Similar to the case of a liquid, the vibrational (phonon) information can be obtained by using the ELNES of a solid. Fig. 7 shows the dependence of temperature on the Al-K edge of alumina (α-Al_2O_3) observed using X-rays [72]. As can be seen from the figure, a sharp and intense peak A appears at the spectrum threshold and a plateau profile appears after peak A. At 930 K, however, small but

Please cite this article as: T. Mizoguchi et al., Excitonic, vibrational, and van der Waals interactions in electron energy loss spectroscopy, Ultramicroscopy (2017), http://dx.doi.org/10.1016/j.ultramic.2017.03.003

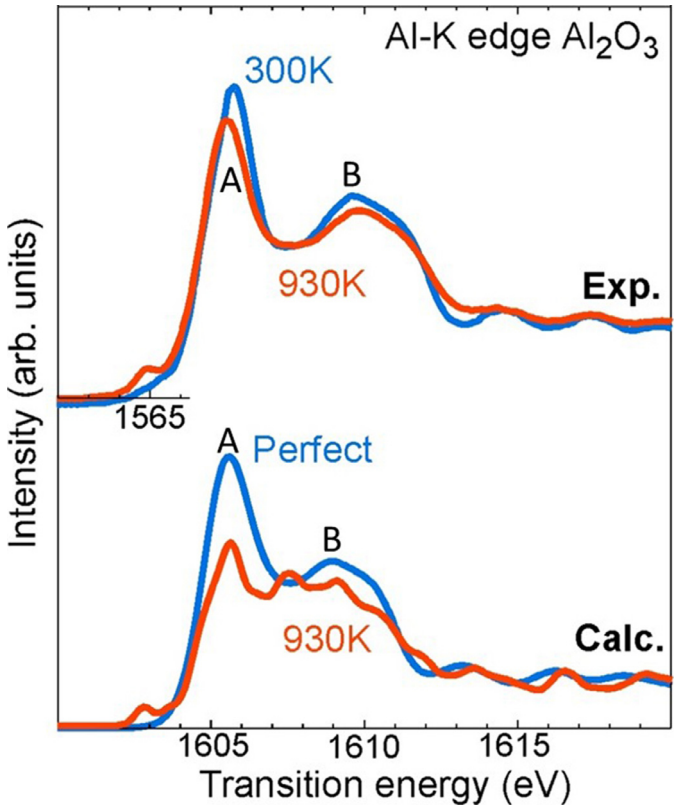

Fig. 7. Effect of temperature on the Al-K edge of Al_2O_3. Experimental spectra were observed using X-rays [72].

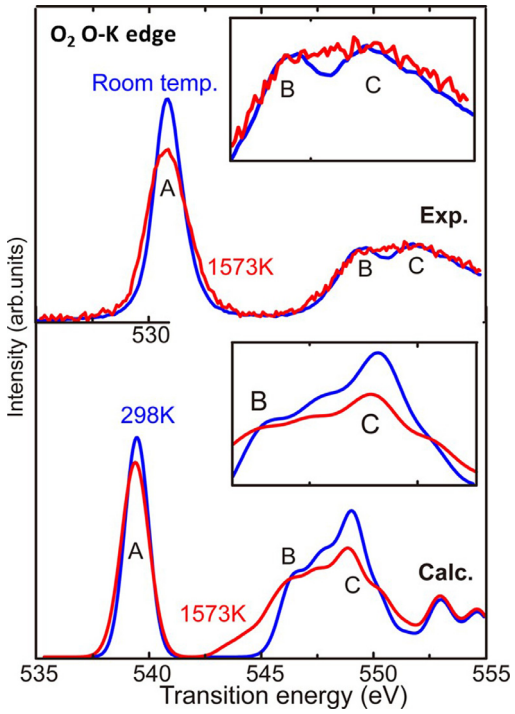

Fig. 8. Effect of temperature on the O-K edge of oxygen gas. The experimental spectra were observed using environmental TEM under an oxygen atmosphere of 15 Pa. Both spectra at room temperature and high temperature are shown.

distinct changes are observed, with a small pre-peak appearing on the lower energy side of peak A and the intensity of peak A being less intense.

To investigate the spectral differences with temperature, a first-principles MD simulation was performed for alumina at 930 K using the CASTEP code. The simulation was performed for the primitive cell (four Al sites) but symmetry constraints were not considered in the simulation to identify the effect of the vibration at each atomic site. One snapshot was taken from the MD simulation, and the Al-K edge spectra for all four Al sites in the primitive cell were calculated. The ELNES calculation was performed using the CASTEP code by expanding the primitive cell to $2 \times 2 \times 2$. Namely, an 80 atoms supercell was used. Four atomic sites were separately calculated and the averaged Al-K edge spectra for all Al sites were compared with the Al-K edge of perfect Al_2O_3 (Fig. 7).

As can be seen in the figure, the spectral changes in the experiment, that is, the pre-peak appearing at the lower energy side of peak A and the decrease of the intensity of peak A, are well reproduced by the present calculations. The calculation analysis revealed that the spectral changes were caused by the symmetry breaking of the Al site by the lattice vibration induced by temperature.

4.2.3. Vibrational information in ELNES of a gas: effect of temperature

In addition to the liquid (Fig. 6) and solid (Fig. 7), the vibrational information in ELNES of a gas was investigated. The ELNES spectrum from oxygen gas was observed using an environmental TEM (HF-3300, Hitachi High Tech.) equipped with a differential pumping system. By using this instrument, we can achieve a 15 Pa gas atmosphere near the specimen without the need for separation membranes. In addition to the gas injection, we used a heating holder. The holder had a tungsten-wire heater so that a high temperature atmosphere could be generated. We heated up the holder to 1573 K and the O-K edge was observed close to the heater. By using these instruments, we obtained the oxygen-K edge spectra of oxygen gas at room temperature and high temperature.

The experimental and calculated O-K edge from oxygen gas are shown in Fig. 8. The spectrum shows a very sharp peak A which is followed by a small peak B. The peaks A and B are known to originate from the electron transition to the unoccupied π^* and σ^* molecular orbitals, respectively. The overall profile did not change even in the spectrum at high temperature. However, a detailed inspection showed that the peak A became less intense and wider and the peak B became broader when compared with the spectrum obtained at room temperature.

To account for the effect of the molecular vibration at high temperatures in the ELNES calculation, we performed a MD simulation of the oxygen gas model and the distribution of the O=O bond lengths at room temperature and 1573 K were measured. Additionally, the oxygen-K edge spectra of the oxygen molecules with different O=O bond lengths were calculated separately. The averaged spectrum of 14 molecule configurations is shown in the same figure. It can be seen that the simulated models can reproduce the experimentally observed spectral changes, that is, peak A becomes less intense and wider and peak B becomes broader as compared with the spectrum obtained at the room temperature. This indicates that the spectral changes arose from the stronger vibrations of gas molecules at the high temperature. Namely, the tungsten heater provides the thermal (kinetic) energy to the oxygen gas molecules and the vibration of the gas molecule becomes stronger, which was identified by using the ELNES.

In this section, we presented the observations of the vibrational information from a gas, liquid, and solid using low energy EELS and ELNES. In-situ experiments under atmosphere, liquid, and external field are a recently growing trend in the TEM community. The vibrational information plays an important role for the dynamic behavior of atoms and molecules. Our results suggest that

Please cite this article as: T. Mizoguchi et al., Excitonic, vibrational, and van der Waals interactions in electron energy loss spectroscopy, Ultramicroscopy (2017), http://dx.doi.org/10.1016/j.ultramic.2017.03.003

the TEM/STEM-EELS method would be a very powerful tool for the investigation of such vibrational information.

Summary

Here, inspired by the great achievements of Ondrej L. Krivanek and his collaborators, we discussed new potential applications of EELS, based on theoretical calculations. First is the excitonic interaction in ELNES. Especially, we have presented the strong excitonic interaction at the relatively high energy O-K edges (~530 eV) of perovskite oxides, and showed that the strong excitonic interaction is present even at the O-K edge owing to the dimensionally confined atomic structure of perovskite oxides. In addition, the importance of the estimation of the transition energy was presented when we wish to apply the excitonic calculation to battery materials. In particular, we presented the results on the Li-K and Fe-$M_{2,3}$ edges of $LiFePO_3$.

The effect of the van der Waals (vdW) interaction in ELNES was also investigated. The magnitude of the vdW effect is approximately 0.1 eV in the case of the ELNES from a solid and liquid. However, the vdW effect is almost negligible in the case of the ELNES from a gas owing to the long inter-molecular distance.

Furthermore, we demonstrated that the acquisition of the infrared spectrum is possible by combination of EELS with a modern monochromator system. In addition to such a direct observation of the infrared spectrum, we demonstrated that measurement of the vibrational information is also possible even in core-loss, namely ELNES. We showed that the spectral features change as a result of atomistic vibrations, allowing the observation of vibrational information from liquid methanol and acetic acid, solid Al_2O_3, and oxygen gas.

Throughout this manuscript, we presented the "new" potential of EELS to investigate the excitonic interaction, vdW interaction, and vibrational information. All of our results suggest that the TEM/STEM-EELS method would be a very powerful tool to explore these new frontiers. However, we would like to emphasize that the correct calculation of the spectrum using a suitable theoretical framework is indispensable to obtain such "frontier" information. We believe that additional new fields will be opened by combining the TEM/STEM-EELS and theoretical calculations.

Acknowledgements

This study was supported by Mitsubishi Science Foundation (27143), Grant-in-Aids for Scientific Research from MEXT (Nos. 25106003, 26630302, 26249092), a Grant-in-Aid from the Japan Society for the Promotion of Science (JSPS) Fellows (No. 15J11146), and JST-PRESTO. The study using the monochromated STEM-EELS was performed by a collaboration with M. Mukai and E. Okunishi, JEOL Ltd., and the study on the gas ELNES was performed by a collaboration with M. Shirai and H. Matsumoto, Hitachi High Tech. Corp. The studies on the BSE-GGA calculation, vdW interaction, and gas ELNES were collaborated with K. Tomita and H. Katsukura, Univ. Tokyo. All authors acknowledge all of these collaborations. W.O. acknowledges support from the Swedish Government Strategic Research Area in Materials Science on Functional Materials at Linköping University (Faculty Grant SFO-Mat-LiU No 2009 00971) and Knut and Alice Wallenbergs Foundation project Strong Field Physics and New States of Matter 2014–2019 (COTXS).

References

[1] R.F. Egerton, Electron Energy-Loss Spectroscopy in the Electron Microscope, Springer US, Boston, MA, 2011, doi:10.1007/978-1-4419-9583-4.
[2] N.D. Browning, M.F. Chisholm, S.J. Pennycook, Atomic-resolution chemical analysis using a scanning transmission electron microscope, Nature 366 (1993) 143–146, doi:10.1038/366143a0.
[3] P.E. Batson, Simultaneous STEM imaging and electron energy-loss spectroscopy with atomic-column sensitivity, Nature 366 (1993) 727–728, doi:10.1038/366727a0.
[4] L.M. Brown, Brown1993.pdf, Nature 366 (1993) 721–721.
[5] D.A. Muller, Y. Tzou, R. Raj, J. Silcox, Mapping sp2 and sp3 states of carbon at sub-nanometre spatial resolution, Nature 366 (1993) 725–727, doi:10.1038/366725a0.
[6] O.L. Krivanek, N. Dellby, A.R. Lupini, Towards sub-Å electron beams, Ultramicroscopy 78 (1999) 1–11, doi:10.1016/S0304-3991(99)00013-3.
[7] P.E. Batson, N. Dellby, O.L. Krivanek, Sub-ångstrom resolution using aberration corrected electron optics, Nature 418 (2002) 617–620, doi:10.1038/nature01058.
[8] O.L. Krivanek, P.D. Nellist, N. Dellby, M.F. Murfitt, Z. Szilagyi, Towards sub-0.5 Å electron beams, Ultramicroscopy 96 (2003) 229–237, doi:10.1016/S0304-3991(03)00090-1.
[9] M. Varela, S.D. Findlay, A.R. Lupini, H.M. Christen, A.Y. Borisevich, N. Dellby, O.L. Krivanek, P.D. Nellist, M.P. Oxley, L.J. Allen, S.J. Pennycook, Spectroscopic imaging of single atoms within a bulk solid, Phys. Rev. Lett. 92 (2004) 95502, doi:10.1103/PhysRevLett.92.095502.
[10] P.D. Nellist, M.F. Chisholm, N. Dellby, O.L. Krivanek, M.F. Murfitt, Z.S. Szilagyi, A.R. Lupini, A. Borisevich, W.H. Sides, S.J. Pennycook, Direct sub-angstrom imaging of a crystal lattice, Science 305 (2004) 1741, doi:10.1126/science.1100965.
[11] O.L. Krivanek, M.F. Chisholm, V. Nicolosi, T.J. Pennycook, G.J. Corbin, N. Dellby, M.F. Murfitt, C.S. Own, Z.S. Szilagyi, M.P. Oxley, S.T. Pantelides, S.J. Pennycook, Atom-by-atom structural and chemical analysis by annular dark-field electron microscopy, Nature 464 (2010) 571–574, doi:10.1038/nature08879.
[12] D.B. Williams, C.B. Carter, Transmission Electron Microscopy, Springer US, Boston, MA, 2009, doi:10.1007/978-0-387-76501-3.
[13] K. Kimoto, T. Asaka, T. Nagai, M. Saito, Y. Matsui, K. Ishizuka, Element-selective imaging of atomic columns in a crystal using STEM and EELS, Nature 450 (2007) 702–704, doi:10.1038/nature06352.
[14] D.A. Muller, L.F. Kourkoutis, M. Murfitt, J.H. Song, H.Y. Hwang, J. Silcox, N. Dellby, O.L. Krivanek, Atomic-scale chemical imaging of composition and bonding by aberration-corrected microscopy, Science 319 (2008) 1073–1076 (80-.), doi:10.1126/science.1148820.
[15] T. Tohei, T. Mizoguchi, H. Hiramatsu, Y. Kamihara, H. Hosono, Y. Ikuhara, Direct imaging of doped fluorine in $LaFeAsO_{1-x}F_x$ superconductor by atomic scale spectroscopy, Appl. Phys. Lett. 95 (2009) 193107, doi:10.1063/1.3263148.
[16] H. Tan, S. Turner, E. Yücelen, J. Verbeeck, G. Van Tendeloo, 2D Atomic mapping of oxidation states in transition metal oxides by scanning transmission electron microscopy and electron energy-loss spectroscopy, Phys. Rev. Lett. 107 (2011) 107602, doi:10.1103/PhysRevLett.107.107602.
[17] J. Verbeeck, H. Tian, P. Schattschneider, Production and application of electron vortex beams, Nature 467 (2010) 301–304, doi:10.1038/nature09366.
[18] P. Schattschneider, S. Rubino, C. Hebert, J. Rusz, J. Kunes, P. Novák, E. Carlino, M. Fabrizioli, G. Panaccione, G. Rossi, Detection of magnetic circular dichroism using a transmission electron microscope, Nature 441 (2006) 486–488, doi:10.1038/nature04778.
[19] B.J. McMorran, A. Agrawal, I.M. Anderson, A.A. Herzing, H.J. Lezec, J.J. McClelland, J. Unguris, Electron vortex beams with high quanta of orbital angular momentum, Science 331 (2011) 192–195, doi:10.1126/science.1198804.
[20] S. Lazar, G.A. Botton, M.Y. Wu, F.D. Tichelaar, H.W. Zandbergen, Materials science applications of HREELS in near edge structure analysis and low-energy loss spectroscopy, Ultramicroscopy 96 (2003) 535–546, doi:10.1016/S0304-3991(03)00114-1.
[21] C. Mitterbauer, G. Kothleitner, W. Grogger, H. Zandbergen, B. Freitag, P. Tiemeijer, F. Hofer, Electron energy-loss near-edge structures of 3d transition metal oxides recorded at high-energy resolution, Ultramicroscopy 96 (2003) 469–480, doi:10.1016/S0304-3991(03)00109-8.
[22] M. Terauchi, M. Tanaka, Development of a high energy resolution electron energy-loss spectroscopy microscope, J. Microsc. 194 (1999) 203–209. http://onlinelibrary.wiley.com/doi/10.1046/j.1365-2818.1999.00450.x/full.
[23] M. Bosman, L.J. Tang, J.D. Ye, S.T. Tan, Y. Zhang, V.J. Keast, Nanoscale band gap spectroscopy on ZnO and GaN-based compounds with a monochromated electron microscope, Appl. Phys. Lett. 95 (2009) 101110, doi:10.1063/1.3222974.
[24] K. Kimoto, Practical aspects of monochromators developed for transmission electron microscopy, Microscopy 63 (2014) 337–344, doi:10.1093/jmicro/dfu027.
[25] O.L. Krivanek, T.C. Lovejoy, N. Dellby, T. Aoki, R.W. Carpenter, P. Rez, E. Soignard, J. Zhu, P.E. Batson, M.J. Lagos, R.F. Egerton, P.A. Crozier, Vibrational spectroscopy in the electron microscope, Nature 514 (2014) 209–212, doi:10.1038/nature13870.
[26] O.L. Krivanek, T.C. Lovejoy, N. Dellby, R.W. Carpenter, Monochromated STEM with a 30 meV-wide, atom-sized electron probe, J. Electron Microsc. 62 (2013) 3–21 (Tokyo), doi:10.1093/jmicro/dfs089.
[27] O.L. Krivanek, T.C. Lovejoy, M.F. Murfitt, G. Skone, P.E. Batson, N. Dellby, Towards sub-10 meV energy resolution STEM-EELS, J. Phys. 522 (2014) 12023, doi:10.1088/1742-6596/522/1/012023.
[28] T. Aoki, L.A.J. Garvie, P. Rez, Observation of color center peaks in calcium fluoride, Ultramicroscopy 153 (2015) 40–44, doi:10.1016/j.ultramic.2015.02.007.
[29] T. Miyata, M. Fukuyama, A. Hibara, E. Okunishi, M. Mukai, T. Mizoguchi, Measurement of vibrational spectrum of liquid using monochromated scanning transmission electron microscopy-electron energy loss spectroscopy, Microscopy 63 (2014) 377–382, doi:10.1093/jmicro/dfu023.

Please cite this article as: T. Mizoguchi et al., Excitonic, vibrational, and van der Waals interactions in electron energy loss spectroscopy, Ultramicroscopy (2017), http://dx.doi.org/10.1016/j.ultramic.2017.03.003

[30] W. Olovsson, I. Tanaka, T. Mizoguchi, P. Puschnig, C. Ambrosch-Draxl, All-electron Bethe-Salpeter calculations for shallow-core x-ray absorption near-edge structures, Phys. Rev. B. 79 (2009) 41102, doi:10.1103/PhysRevB.79.041102.
[31] G. Onida, L. Reining, A. Rubio, Electronic excitations: density-functional versus many-body Green's-function approaches, Rev. Mod. Phys. 74 (2002) 601–659, doi:10.1103/RevModPhys.74.601.
[32] J.J. Rehr, J.A. Soininen, E.L. Shirley, FinalState rule vs the BetheSalpeter equation for DeepCore xray absorption spectra, Phys. Scr. 2005 (2005) 207, doi:10.1238/Physica.Topical.115a00207.
[33] E.L. Shirley, Local screening of a core hole: a real-space approach applied to hafnium oxide, Ultramicroscopy 106 (2006) 986–993, doi:10.1016/j.ultramic.2006.05.008.
[34] J. Vinson, J.J. Rehr, J.J. Kas, E.L. Shirley, Bethe-Salpeter equation calculations of core excitation spectra, Phys. Rev. B. 83 (2011) 115106, doi:10.1103/PhysRevB.83.115106.
[35] T. Mizoguchi, W. Olovsson, H. Ikeno, I. Tanaka, Theoretical ELNES using one-particle and multi-particle calculations, Micron 41 (2010) 695–709, doi:10.1016/j.micron.2010.05.011.
[36] K. Tomita, T. Miyata, W. Olovsson, T. Mizoguchi, Strong excitonic interactions in the oxygen K-edge of perovskite oxides, Ultramicroscopy (2016) 1–7, doi:10.1016/j.ultramic.2016.04.006.
[37] K. Tomita, T. Miyata, W. Olovsson, T. Mizoguchi, Core-exciton interaction in sodium L2,3 edge structure investigated using the Bethe-Salpeter equation, J. Phys. Chem. C. 120 (2016) 9036–9042, doi:10.1021/acs.jpcc.5b12389.
[38] K. van Benthem, G. Tan, L.K. DeNoyer, R.H. French, M. Rühle, Local optical properties, electron densities, and london dispersion energies of atomically structured grain boundaries, Phys. Rev. Lett. 93 (2004) 227201, doi:10.1103/PhysRevLett.93.227201.
[39] H. Katsukura, T. Miyata, K. Tomita, T. Mizoguchi, Effect of the van der Waals interaction on the electron energy-loss near edge structure theoretical calculation, Ultramicroscopy (2016) 0–1, doi:10.1016/j.ultramic.2016.07.012.
[40] Y. Matsui, T. Mizoguchi, First principles calculation of oxygen K edge absorption spectrum of acetic acid: Relationship between the spectrum and molecular dynamics, Chem. Phys. Lett. 649 (2016) 92–96, doi:10.1016/j.cplett.2016.02.043.
[41] Y. Matsui, K. Seki, A. Hibara, T. Mizoguchi, An estimation of molecular dynamic behaviour in a liquid using core-loss spectroscopy, Sci. Rep. 3 (2013) 1–7, doi:10.1038/srep03503.
[42] Y. Noguchi, M. Hiyama, H. Akiyama, Y. Harada, N. Koga, First-principles investigation of strong excitonic effects in oxygen 1 s X-ray absorption spectra, J. Chem. Theory Comput. 11 (2015) 1668–1673, doi:10.1021/acs.jctc.5b00082.
[43] C. Hébert, Practical aspects of running the WIEN2k code for electron spectroscopy, Micron 38 (2007) 12–28, doi:10.1016/j.micron.2006.03.010.
[44] P. Blaha, K. Schwarz, G.K.H. Madsen, D. Kvasnicka, J. Luitz, WIEN2k, an augmented plane Wave+Local orbitals program for calculating crystal properties, (2001).
[45] S. Nakai, T. Sagawa, Na^{+}L2,3 edge absorption spectra of sodium halides, J. Phys. Soc. JAPAN (1969) 26.
[46] S. Kobayashi, C.A.J. Fisher, T. Kato, Y. Ukyo, T. Hirayama, Y. Ikuhara, Atomic-scale observations of (010) $LiFePO_4$ surfaces before and after chemical delithiation, Nano Lett. (2016) acs.nanolett.6b01689, doi:10.1021/acs.nanolett.6b01689.
[47] Y. Koyama, T. Mizoguchi, H. Ikeno, I. Tanaka, Electronic structure of lithium nickel oxides by electron energy loss spectroscopy, J. Phys. Chem. B. 109 (2005) 10749–10755, doi:10.1021/jp050486b.
[48] K. Kubobuchi, M. Mogi, H. Ikeno, I. Tanaka, H. Imai, T. Mizoguchi, Mn L2,3-edge X-ray absorption spectroscopic studies on charge-discharge mechanism of Li_2MnO_3, Appl. Phys. Lett. 104 (2014) 53906, doi:10.1063/1.4864167.
[49] K. Kubobuchi, M. Mogi, M. Matsumoto, T. Baba, C. Yogi, C. Sato, T. Yamamoto, T. Mizoguchi, H. Imai, A valence state evaluation of a positive electrode material in an Li-ion battery with first-principles K- and L-edge XANES spectral simulations and resonance photoelectron spectroscopy, J. Appl. Phys. 120 (2016) 142125, doi:10.1063/1.4963379.
[50] P. Moreau, F. Boucher, Revisiting lithium K and iron M 2,3 edge superimposition: the case of lithium battery material $LiFePO_4$, Micron 43 (2012) 16–21, doi:10.1016/j.micron.2011.05.008.
[51] E.L. Shirley, Li 1s near-edge spectra in six lithium halides, J. Electron Spectrosc. Relat. Phenom. 137–140 (2004) 579–584, doi:10.1016/j.elspec.2004.02.050.
[52] K. Persson, Materials Data on $LiFePO_4$ (SG:74) by Materials Project, 2014, doi:10.17188/1301164.
[53] H. Ikeno, T. Mizoguchi, Y. Koyama, Z. Ogumi, Y. Uchimoto, I. Tanaka, Theoretical fingerprints of transition metal L2,3 XANES and ELNES for lithium transition metal oxides by ab initio multiplet calculations, J. Phys. Chem. C. 115 (2011) 11871–11879, doi:10.1021/jp202383n.
[54] Hi. Ikeno, I. Tanaka, Effects of Breit interaction on the L_{2,3} x-ray absorption near-edge structures of 3d transition metals, Phys. Rev. B. 77 (2008) 75127, doi:10.1103/PhysRevB.77.075127.
[55] W.-Y. Ching, P. Rulis, X-ray absorption near edge structure/electron energy loss near edge structure calculation using the supercell orthogonalized linear combination of atomic orbitals method, J. Phys. Condens. Matter. 21 (2009) 104202, doi:10.1088/0953-8984/21/10/104202.
[56] C. Hébert, J. Luitz, P. Schattschneider, Improvement of energy loss near edge structure calculation using Wien2k, Micron 34 (2003) 219–225, doi:10.1016/S0968-4328(03)00030-1.
[57] T. Mizoguchi, I. Tanaka, S. Yoshioka, M. Kunisu, T. Yamamoto, W.Y. Ching, First-principles calculations of ELNES and XANES of selected wide-gap materials: dependence on crystal structure and orientation, Phys. Rev. B. 70 (2004) 45103, doi:10.1103/PhysRevB.70.045103.
[58] C. Elsa, S. Ko, Ab initio calculation of near-edge structures in electron-energy-loss spectra for metal-oxide crystals, Phys. Rev. B. 60 (1999) 25–34, doi:10.1103/PhysRevB.60.14025.
[59] N.R. Lugg, M. Haruta, M.J. Neish, S.D. Findlay, T. Mizoguchi, K. Kimoto, L.J. Allen, Removing the effects of elastic and thermal scattering from electron energy-loss spectroscopic data, Appl. Phys. Lett. 101 (2012) 183112, doi:10.1063/1.4765657.
[60] M. Haruta, T. Nagai, N.R. Lugg, M.J. Neish, M. Nagao, K. Kurashima, L.J. Allen, T. Mizoguchi, K. Kimoto, Atomic resolution chemical bond analysis of oxygen in La_2CuO_4, J. Appl. Phys. 114 (2013) 83712, doi:10.1063/1.4819397.
[61] M.J. Neish, N.R. Lugg, S.D. Findlay, M. Haruta, K. Kimoto, L.J. Allen, Detecting the direction of oxygen bonding in $SrTiO_3$, Phys. Rev. B. 88 (2013) 115120, doi:10.1103/PhysRevB.88.115120.
[62] S. Kawanishi, T. Mizoguchi, Effect of van der Waals interactions on the stability of SiC polytypes, J. Appl. Phys. 119 (2016) 175101-1-4, doi:10.1063/1.4948329.
[63] A. Tkatchenko, M. Scheffler, Accurate molecular van der Waals interactions from ground-state electron density and free-atom reference data, Phys. Rev. Lett. 102 (2009) 73005, doi:10.1103/PhysRevLett.102.073005.
[64] S.J. Clark, M.D. Segall, C.J. Pickard, P.J. Hasnip, M.I.J. Probert, K. Refson, M.C. Payne, First principles methods using CASTEP, Zeitschrift Fur Krist 220 (2005) 567–570, doi:10.1524/zkri.220.5.567.65075.
[65] X. Chu, A. Dalgarno, Molecular transition moments at large internuclear distances, Phys. Rev. A. 66 (2002) 24701, doi:10.1103/PhysRevA.66.024701.
[66] F.L. Hirshfeld, Difference densities by least-squares refinement: fumaramic acid, Acta Crystallogr. Sect. B Struct. Crystallogr. Cryst. Chem. 27 (1971) 769–781, doi:10.1107/S0567740871002905.
[67] J. Perdew, K. Burke, M. Ernzerhof, Phys Rev Lett 77 (1996) 3865 Errata(1997) Phys Rev Lett.
[68] T. Mizoguchi, I. Tanaka, S.-P. Gao, C.J. Pickard, First-principles calculation of spectral features, chemical shift and absolute threshold of ELNES and XANES using a plane wave pseudopotential method, J. Phys. Condens. Matter. 21 (2009) 104204, doi:10.1088/0953-8984/21/10/104204.
[69] T. Mizoguchi, K. Matsunaga, E. Tochigi, Y. Ikuhara, First principles pseudopotential calculation of electron energy loss near edge structures of lattice imperfections, Micron 43 (2012) 37–42, doi:10.1016/j.micron.2011.07.005.
[70] P.A. Crozier, T. Aoki, Q. Liu, Detection of water and its derivatives on individual nanoparticles using vibrational electron energy-loss spectroscopy, Ultramicroscopy 169 (2016) 30–36 Author's Accepted Manuscript spectroscopy, doi:10.1016/j.ultramic.2016.06.008.
[71] P. Rez, T. Aoki, K. March, D. Gur, O.L. Krivanek, N. Dellby, T.C. Lovejoy, S.G. Wolf, H. Cohen, Damage-free vibrational spectroscopy of biological materials in the electron microscope, Nat. Commun. 7 (2016) 10945, doi:10.1038/ncomms10945.
[72] D. Manuel, D. Cabaret, C. Brouder, P. Sainctavit, A. Bordage, N. Trcera, Experimental evidence of thermal fluctuations on the x-ray absorption near-edge structure at the aluminum K edge, Phys. Rev. B. 85 (2012) 224108–224113, doi:10.1103/PhysRevB.85.224108.
[73] T. Mizoguchi, J.P. Buban, K. Matsunaga, T. Yamamoto, Y. Ikuhara, First-principles study on incidence direction, individual site character, and atomic projection dependences of ELNES for perovskite compounds, Ultramicroscopy 106 (2006) 92–104, doi:10.1016/j.ultramic.2005.06.006.
[74] T. Mizoguchi, K. Tatsumi, I. Tanaka, Peak assignments of ELNES and XANES using overlap population diagrams, Ultramicroscopy 106 (2006) 1120–1128, doi:10.1016/j.ultramic.2006.04.027.
[75] T. Mizoguchi, Study on atomic and electronic structures of ceramic materials using spectroscopy, microscopy, and first principles calculation, J. Ceram. Soc. Japan. 119 (2011) 325–333, doi:10.2109/jcersj2.119.325.
[76] K.R. Wilson, J.G. Tobin, A.L. Ankudinov, J.J. Rehr, R.J. Saykally, Extended X-Ray absorption fine structure from hydrogen atoms in water, Phys. Rev. Lett. 85 (2000) 4289–4292, doi:10.1103/PhysRevLett.85.4289.
[77] K.R. Wilson, M. Cavalleri, B.S. Rude, R.D. Schaller, T. Catalano, A. Nilsson, R.J. Saykally, L.G.M. Pettersson, X-ray absorption spectroscopy of liquid methanol microjets: bulk electronic structure and hydrogen bonding network, J. Phys. Chem. B. 109 (2005) 10194–10203, doi:10.1021/jp049278u.
[78] M. Jaouen, G. Hug, V. Gonnet, G. Demazeau, G. Tourillon, An EELS and XAS study of cubic boron nitride synthesized under high pressure - high temperature conditions, Microsc. Microanal. Microstruct. 6 (1995) 127–139, doi:10.1051/mmm:1995113.
[79] M. Nagasaka, K. Mochizuki, V. Leloup, N. Kosugi, Local structures of methanol-water binary solutions studied by soft X-ray absorption spectroscopy, J. Phys. Chem. B. 118 (2014) 4388–4396, doi:10.1021/jp4091602.
[80] T. Tokushima, Y. Horikawa, Y. Harada, O. Takahashi, A. Hiraya, S. Shin, Selective observation of the two oxygen atoms at different sites in the carboxyl group (-COOH) of liquid acetic acid., Phys. Chem. Chem. Phys. 11 (2009) 1679–1682, doi:10.1039/b818812b.

Please cite this article as: T. Mizoguchi et al., Excitonic, vibrational, and van der Waals interactions in electron energy loss spectroscopy, Ultramicroscopy (2017), http://dx.doi.org/10.1016/j.ultramic.2017.03.003